frontiers | Frontiers in Materials

TYPE Original Research
PUBLISHED 30 May 2024
DOI 10.3389/fmats.2024.1390372

OPEN ACCESS

EDITED BY
Babatunde Okesola,
University of Nottingham, United Kingdom

REVIEWED BY
Dhakshinamoorthy Sundaramurthi,
SASTRA University, India
Kristine Salma-Ancane,
Riga Technical University, Latvia

*CORRESPONDENCE
Yadong Zhang,
drzyd@126.com
Yantao Zhao,
userzyt@qq.com

†These authors have contributed equally to this work

RECEIVED 23 February 2024
ACCEPTED 13 May 2024
PUBLISHED 30 May 2024

CITATION
Ma H, Xie B, Chen H, Song P, Zhou Y, Jia H, Liu J, Zhao Y and Zhang Y (2024), High-strength and high-elasticity silk fibroin-composite gelatin biomaterial hydrogels for rabbit knee cartilage regeneration.
Front. Mater. 11:1390372.
doi: 10.3389/fmats.2024.1390372

High-strength and high-elasticity silk fibroin-composite gelatin biomaterial hydrogels for rabbit knee cartilage regeneration

Hebin Ma[1,2,3†], Bowen Xie[4†], Hongguang Chen[2,3†], Puzhen Song[1], Yuanbo Zhou[1], Haigang Jia[2], Jing Liu[5], Yantao Zhao[2,3*] and Yadong Zhang[2,6*]

[1]Medical School of Chinese PLA, Beijing, China, [2]Senior Department of Orthopedics, the Fourth Medical Center of PLA General Hospital, Beijing, China, [3]Beijing Engineering Research Center of Orthopedics Implants, Beijing, China, [4]Air Force Clinical College, The Fifth School of Clinical Medicine, Anhui Medical University Beijing, Beijing, China, [5]Department of Radiological, the Fourth Medical Center of PLA General Hospital, Beijing, China, [6]Department of Orthopedics, the Fifth Medical Center of PLA General Hospital, Beijing, China

Suitable hydrogel materials for cartilage tissue repair should exhibit high strength and toughness, and excellent biocompatibility. However, the mechanical properties of most hydrogels cannot meet the complex mechanical requirements of articular cartilage tissues. Given this situation, we have adopted a chemical cross-linking method using hexafluoro isopropanol to mediate the cross-linking of Silk Fibroin (SF) and deionized water (DI), which promoted the formation of β-sheets, generating "high-toughness" Silk Fibroin hydrogels. The introduction of Gelatin (Gel) served to increase the content of β-sheets and increase the tensile modulus from 24.51 ± 2.07 MPa to 39.75 ± 6.54 MPa, which significantly enhanced the flexibility of the hydrogel and meets the mechanical requirements of cartilage tissue. In addition, *in vitro* biological experiments have shown that the introduction of Gel promotes cell proliferation and enhances the production of cartilage extracellular matrix by chondrocytes. *In vivo* experiments have demonstrated that SF/Gel hydrogel promotes articular cartilage regeneration more effectively than SF hydrogel, as evidenced by improvements in gross appearance, imaging, and histology. This study has established that high-strength SF/Gel hydrogel prepared by applying the binary-solvent-induced conformation transition strategy has potential applications in cartilage tissue repair and regeneration and is a feasible biomaterial for osteochondral regeneration.

KEYWORDS

hydrogel, cartilage repair, gelatin, silk fibroin, high elasticity

1 Introduction

Cartilage is a hydrogel-like structure with a significant water content, and is rich in collagen and glycosaminoglycan (GAG) polymers, exhibiting mechanical properties that meet the necessary compressive and tensile demands of joint movement (Sánchez-Téllez et al., 2017). Cartilage damage is a common health issue worldwide, caused by a variety of factors, such as aging, obesity and mechanical injury (Krishnan and Grodzinsky, 2018). Mature articular cartilage lacks nerve and blood flow, resulting in late detection of

damage and difficulty in healing (Liu et al., 2018; Zhang et al., 2019b). If left untreated, the injury can lead to irreversible degeneration of the joints, resulting in osteoarthritis and ultimately disability (Chen et al., 2009). There are many new types of surgical treatments for cartilage injuries, which include microfracture, arthroscopic techniques, cartilage grafting and chondrocyte transplantation. However, none of these methods enable long-term therapeutic treatment and cannot effectively treat cartilage injuries (Zhang et al., 2019a; Chahla et al., 2019; Le et al., 2020). Consequently, it is urgent for effective treatments for cartilage injuries.

The development of tissue engineering has shown promise in providing a solution to the challenge of cartilage damage (Le et al., 2020). Cartilage tissue engineering can provide an ideal microenvironment for cell growth and promote extracellular matrix (ECM) deposition (Wubneh et al., 2018; Cui et al., 2023). It can serve as an effective treatment of cartilage damage, slowing the progression of osteoarthritis (Wubneh et al., 2018; Shi et al., 2019; Cui et al., 2023; Ni et al., 2023). Hydrogel is one of the scaffolds commonly used in tissue engineering. It has a three-dimensional hydrophilic network with high water content and porosity, and is similar to cartilage tissue in structure (Zhang et al., 2021). Hydrogel materials are broadly classified into two categories: biomaterial hydrogel and synthetic hydrogel. Biomaterial hydrogel exhibit outstanding biocompatibility, fostering cell proliferation and ECM synthesis. Nonetheless, their biomechanical characteristics are somewhat lacking (Sheehy et al., 2015; Thomas and Mercuri, 2023). Examples of such materials are Silk Fibroin (SF) (Gong et al., 2020), Gelatin (Gel) (Wu et al., 2020), Chitosan (Luo et al., 2022), Sodium Alginate (Luo et al., 2022) and Cellulose (Zhu X. et al., 2018). Synthetic hydrogels possess exceptional biomechanical properties that can fulfill the mechanical demands of articular cartilage. Nevertheless, they exhibit a lack of biocompatibility and have the potential to generate toxic metabolites that hinder cell proliferation and ECM production (Sheehy et al., 2015; Thomas and Mercuri, 2023). These materials include Polyvinyl Alcohol (Li et al., 2019; Gan et al., 2020), Polyacrylamide (Buyanov et al., 2019; Awasthi et al., 2021), Polyethylene Glycol (Schneider et al., 2019) and Polyvinylpyrrolidone (Li et al., 2022). An ideal hydrogel should exhibit the following advantages: excellent mechanical properties, high porosity, and good biocompatibility (Zhou et al., 2023). The primary challenge lies in developing hydrogels with superior mechanical properties without compromising biocompatibility for effective cartilage tissue regeneration and repair. Therefore, we are dedicated to developing a biomaterial hydrogel with superior biomechanical properties and excellent biocompatibility.

SF protein, as a natural biomaterial derived from *Bombyx mori*, is FDA approved and widely used in clinical treatment. Some studies have shown that SF protein has excellent mechanical properties and good biocompatibility (Zhang et al., 2018). The biomechanical strength of SF hydrogels is related to the number of β-sheets and their orientation (De Leon Rodriguez et al., 2016; Su et al., 2017). Most studies indicate that SF hydrogels typically exhibit poor biomechanical properties, a fragile and brittle texture, and limited loading capacity (Kapoor and Kundu, 2016). While methods such as chemical or enzymatic cross-linking can improve mechanical strength, achieving biomaterial hydrogels with both high strength and toughness that meet the mechanical demands of articular cartilage continues to be a significant challenge. Gel is a prevalent protein formed by the degradation of the triple-helical structure of collagen into single-stranded macromolecules. Gel is the main single-chain derivative of collagen in the cartilage matrix, with a large number of natural molecular epitopes that maintain cell adhesion and signal transduction, increasing cell proliferation and cartilage matrix production, and facilitating a range of biological functions. Moreover, they can promote the formation of β-sheets, which serve to increase the mechanical properties of hydrogels (Lien et al., 2009; Zhu and Marchant, 2011; Zhang et al., 2018; Abpeikar et al., 2021).

In this study, a biomaterial hydrogel was successfully developed by combining SF and Gel biomaterials, showcasing exceptional mechanical properties and biocompatibility. The work has involved an assessment of the physicochemical properties, mechanical properties and biocompatibility of SF hydrogels and SF/Gel hydrogel, with an evaluation of therapeutic efficacy in cartilage regeneration using a cartilage-deficient large white rabbit model (Figure 1).

2 Materials and methods

2.1 Preparation of hydrogels

Preparation of SF proteins. SF was chemically extracted from *B. mori* using lithium bromide (LiBr) (Rockwood et al., 2011). Sodium carbonate (CAS:497-19-8 Aladdin China) solution (0.5 wt%) was used in a 50:1 ratio for degumming. The silk fiber was boiled twice at 95°C for 30 min each time, then washed with distilled water and dried. The resulting silk fiber was dissolved in 9.3 M LiBr (CAS:7550-35-8 Aladdin China) at 60°C for 2 h to create a 20wt% silk fibroin solution. This solution was then filtered through eight layers of gauze. The dissolved silk fibers underwent dialysis in distilled water using a dialysis membrane (8 kDa Solarbio China) and were subsequently freeze-dried.

High-strength and high-elasticity SF hydrogels were prepared utilizing the binary-solvent-induced conformation transition (BSICT) strategy (Zhu Z. et al., 2018), wherein a sample of SF protein (0.8 g) was dissolved in 3 mL hexafluoro isopropanol (HFIP) (CAS:920-66-1 Aladdin China) and stirred for 30 min. Once the SF protein had completely dissolved, 1.5 mL of deionized water (DI) or 1.5 mL of a 2% Gel aqueous solution (CAS: 9000-70-8 Sinopharm China) was added. The mixture was then transferred to an airtight container and incubated at 48°C overnight. According to previous studies (Zhu Z. et al., 2018), the boiling method was found to be effective in removing HFIP. The hydrogel was then transferred to DI and boiled for 2 h, divided into two groups: Before and After. In the aforementioned preparation process, the addition of DI is denoted as SF hydrogel, while the incorporation of a 2% Gel aqueous solution is labeled as SF/Gel hydrogel. Both groups represent samples post-boiling.

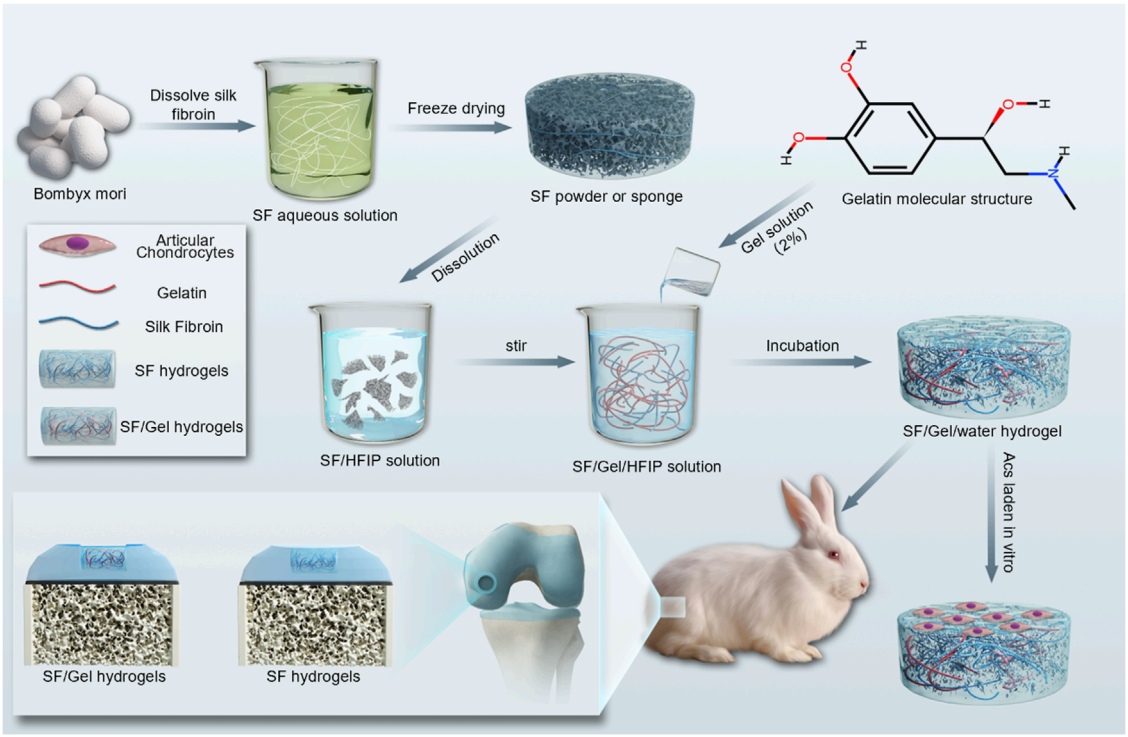

FIGURE 1
Schematic representation of the scope of this study.

2.2 Hydrogel physicochemical properties

2.2.1 Scanning electron microscopy (SEM)

The morphology of two sets of freeze-dried hydrogel scaffolds were characterized by SEM (Verios G4 UC, Thermo United States). 5 pores were randomly measured in each scaffold to determine the pore size by ImageJ software (NIH, Bethesda, MD United States).

2.2.2 Water content test

The water content was determined by gravimetric method. This involved measuring the wet weight (W1) of the two groups of hydrogels (the test was repeated for five samples taken from each group to determine the average water contents), then freeze-drying the samples and measuring the dry weight (W0) (Sornkamnerd et al., 2017):

$$\textbf{Water content}(\%) = (W1 - W0)/W1 * 100\%$$

2.2.3 Fourier transform infrared (FTIR) spectral analysis

To investigate the changes in chemical bonding and the effect of HFIP removal during hydrogel preparation, samples (SF protein, Gel protein, Before, After, SF hydrogel and SF/Gel hydrogel) underwent analysis using an FTIR spectrometer (Nicolet 6,700, Thermo). The raw data was processed in Origin software for FTIR spectral analysis after chemical cross-linking and HFIP removal. Baseline correction and second-order derivative fitting were then conducted, followed by calculating the ratio of secondary protein structure based on the area of characteristic peaks of each chemical bond.

2.2.4 Mechanical properties

Based on the national standards GB/T 1041-2008 and GB/T 10433-2018, we prepared two groups of hydrogels for biomechanical samples. Compression and tensile tests were carried out in the wet state using a universal mechanical testing machine (Shandong Wanchen China). In the compression test, a cylindrical hydrogel scaffold was prepared (diameter = 14 mm and height = 5 mm) and the test was performed at a compression speed of 5 mm/min until the deformation reached 60%. Repeating for five samples in each group to determine the average compressive modulus. In the tensile test, a rectangular hydrogel scaffold was prepared (length = 40 mm, width = 5 mm, height = 5 mm) and the tensile test was conducted at a speed of 20 mm/min until the hydrogel scaffold became detached. The stress at this point was recorded, and the test was repeated for five samples taken from each group to determine the average tensile modulus.

2.3 *In vitro* evaluation

2.3.1 Cytotoxicity

To assess the biosafety of the hydrogel, we initially evaluated its cytotoxicity towards chondrocytes through the cell counting kit-8 (CCK-8) (Dojindo Japan) assay. The hydrogel extract was prepared in accordance with the ISO 10993-5 and ISO 10993-12 protocols (Fiocco et al., 2017), then utilized for chondrocyte culture

to determine the survival rate of chondrocytes (Budharaju et al., 2024). This involved placing a specific weight (0.2 g/mL) of hydrogel in chondrocyte culture medium (composed of 90% DMEM-F12 medium, 10% FBS, and 1% antibiotics) to obtain the extract. Articular chondrocytes (AC) were seeded in 96-well plates at a density of 5,000 cells/well (with the negative control being chondrocyte medium only) and incubated for approximately 24 h. Following this incubation period, the medium was replaced with hydrogel extract (with the positive control being chondrocyte medium) (n = 5). After 3 days of further incubation, 10ul of CCK-8 solution was added to each well and incubated for 2 h. Cell viability (%) was determined by measuring the absorbance at 450 nm using an enzyme marker (Thermo Fisher United States).

2.3.2 Seeding of AC on hydrogel scaffolds

After sterilization (autoclave sterilization, 122°C, 30 min and 104 kPa), two groups of hydrogels were placed in 24-well plates, in which the hole without hydrogels material was the control group. Rabbit AC of knee joint were isolated and cultured according to the previously reported procedure (Li et al., 2004). The AC were seeded at a density of 5×10^4 cells/well at the top of each hydrogel. Then, 1 mL chondrocyte culture medium was added and the sample was placed in the cell culture incubator, changing the medium every 2–3 days.

2.3.3 Cell viability

The Alamar Blue (Yeasen China) method was used to assess the metabolic activity of AC on the hydrogel scaffolds in both groups. After the cell-hydrogel complexes were cultured in the cell incubator for one, three, five, seven and 14 days, 100 μL alamar blue solution was added to each well of the culture plate, and the incubation continued for a further 6 h. Aspirated 100 μL sample from each well and added to the 96-well culture plate. The optical density (OD) value was measured at the wavelength of 570 nm by enzyme marker, where three samples were analyzed from each group; the sample without hydrogel served as the control group.

2.3.4 Live-dead staining

In order to observe the survival status of the cells on the hydrogels, the cells were stained using the Live/Dead Staining Kit (Beyotime China). After the cell-hydrogel complexes was cultured for 5 days, washing the complex twice with PBS, and added 500 μL Calcein-AM/PI live-dead staining reagent (Beyotime China) to each well. The cells were incubated at 37°C for 30 min in the dark, and then observed under a fluorescence inverted microscope (Olympus Japan). Images of the three sites were collected, and the area of live and dead cells was analyzed using ImageJ software to assess cell survival rate.

2.3.5 Cell adhesion

The morphology of cells on hydrogel scaffolds was assessed using phalloidin-DAPI staining to detect the cell growth status. The cell-hydrogel complexes were cultured for 5 days, rinsed twice with PBS, and fixed with 4% paraformaldehyde for 20 min. The cells were treated with 0.1% Triton X-100 (Aladdin China), and stained with Actin-Tracker Green-488 (Beyotime China) at 37°C for 1 h, washed three times, then stained with DAPI (5ug/mL) for 10 min. The morphology of AC on both scaffolds was visually evaluated using a fluorescence microscope (Olympus Japan).

2.3.6 Biochemical assays for DNA, GAG and collagen

The ability of AC to secrete a cartilage ECM on the two sets of hydrogel scaffolds was evaluated by monitoring the DNA content of the cell-hydrogel complexes. The content of GAG and collagen in the medium taken after three, five, seven and 14 days of cell-hydrogel cultivation was detected, which in combination with the DNA content, provided a measure of GAG and collagen secretion. The cell/scaffold complexes were digested in a mixture of 125 mg/mL papain (Protein≥10 units/mg) (CAS:9001-734 Yangguagbio China), 100 mM Na_2HPO_4 and 5 mM EDTA at 60°C for 16 h (Li et al., 2020). The DNA content was determined using a DNA quantification kit (Yeasen China). As hydroxyproline (HYP) accounts for 13% of collagen, the collagen content was estimated based on HYP content. Following the manufacturer's instructions, the GAG ELISA kit (Nanjing Jiancheng China) and HYP ELISA kit (Solarbio China) were used to determine the content of cell-secreted GAG and HYP in the cell culture solution. A calibration curve employed standard solutions and was used to determine the content of GAG and HYP.

2.3.7 RT-PCR assay analysis

Quantitative RT-PCR was performed with ChamQ universal SYBR qPCR Master Mix reagent (Novartis, China) and ABI QuantStudio 7 Flex Real-Time PCR System (Thermo Fisher, United States) to determine the expression of specific genes (collagen I, collagen II, sox 9, and aggrecan). After 14 days of cell-hydrogel complexes, the specimens were washed twice in PBS and all the mRNA in the cell-hydrogel complexes was extracted using Trizol (Tiangen Biochemistry, China). The mRNA was quantified using a Nano drop spectrophotometer (Efficient Instruments, China). Total RNA was isolated and reverse transcribed into cDNA using the Evo M-MLV Reverse Transcription Premix Kit (Accurate Biology, China). The RT-PCR tests involved cycling for 40 cycles from 95°C for 3 min, 95°C for 10 s, and 60°C for 30 s; GAPDH RNA served as the internal reference gene. The expression of the target genes was quantified using the ΔΔCt method, normalizing the expression of the target genes to the expression of GAPDH RNA. The primers involved are in the supporting information (Supplementary Table S1).

2.4 *In vivo* cartilage repair

2.4.1 Articular cartilage defect

The New Zealand White rabbits in this study were provided by Beijing Keyu Animal Breeding Center, and the experiment was performed under a protocol approved by the Institutional Animal Care and Use Committee of Beijing Keyu (KY20230925005), complying with the guidelines for the Care and Use of Laboratory Animals (National Academies Press, National Institutes of Health Publication No. 85-23, revised 1996). Eighteen male New Zealand Large White rabbits, males, weighing 2.3 ± 0.5 kg, were selected and randomly divided into three groups. The first group was selected as the control group with no implanted material. The second group (SF

hydrogel group) were implanted with SF hydrogel material. The third group (SF/Gel hydrogel group) were implanted with SF/Gel hydrogel material.

First, penicillin (1 × 104 U/kg) was intermuscular injected to prevent infection. Then, anesthesia was induced by intravenous injection of ethyl carbamate (0.2 g/mL) 10 mL into the marginal ear vein. After animals were anesthetized, subcutaneous and fascial incisions were made sequentially along the medial side of the knee joint, and the patella was partially dislocated to expose the medial femoral condyle of the knee. A full-length defect of cartilage with a diameter of 3 mm and depth of 3 mm was drilled. The defect was cleaned with PBS thoroughly, wiped with a sterile gauze and implanted with stent material. The patella was then reset, sutured the surgical wound layer by layer wrapped with sterile gauze after iodine-vapor disinfection. In order to prevent infection, daily penicillin intramuscular injections were enabled for three consecutive days and each rabbit returned to its cage moving voluntarily. All rabbits were euthanized and assessed at 1 and 2 months post-surgery.

2.4.2 Imaging evaluation

One and 2 months after surgery, three rabbits were randomly selected from each group and euthanized by injecting an overdose of anesthetic. The tibia fibula and femur were dissociated and 7.0T Micro-MRI(Bruker Company, Germany) was performed. The cartilage repair was observed from the sagittal position and assessed using the Henderson MRI evaluation criteria (Brown et al., 2004).

2.4.3 Macroscopic view analysis

The knee joint was opened and images of osteochondral defects were taken with a digital camera. Cartilage tissue repair was evaluated in all samples according to the International Cartilage Repair Society (ICRS) Macroscopic Evaluation Scale (Wakitani et al., 1994).

2.4.4 Histology and immunohistochemical analysis

Femoral condyles were taken and fixed in 4% (v/v) paraformaldehyde, decalcified using 10% (w/v) EDTA, dehydrated, paraffin embedded, and then cut to a 7 μm thickness. The extent and quality of new tissue formation were determined using Hematoxylin and Eosin (H&E) staining, Safranin O/Fast greens staining (Saf O-Fg), Sirius red, and Toluidine blue staining. Immunohistochemical staining of COL-II was performed to assess the regeneration of cartilage tissue. The repair tissue assessment was based on the ICRS (Supplementary Table S1) (Mainil-Varlet et al., 2003) score with five observers (unaware of group). The total (maximum) score was 18 with a minimum score of 0, as outlined in Table 2.

2.5 Statistical analysis

Data are expressed as mean ± standard deviation. All statistical analyses were performed using SPSS 26.0 and GraphPad Prism 8.0.2. All statistical analyses employed a Student's t-test, a one-way analysis of variance (ANOVA) and Sidak's two-way ANOVA for multiple comparisons; $p < 0.05$ was considered a statistically significant difference.

3 Results

3.1 Preparation and characterization of SF/Gel hydrogels

3.1.1 SEM, pore sizes and water content analysis

Through general observation, there was no significant difference between the two groups of hydrogels (Figure 2A). The microstructure of the SF hydrogels and SF/Gel hydrogels scaffolds was analyzed by SEM (Figure 2B). It can be seen that the surface of the SF hydrogels and SF/Gel hydrogels scaffolds are rough, with a uniform distribution of pores. Both materials can form a three-dimensional interconnected mesh structure that may serve as a suitable microenvironment for the exchange of compounds in cells. Taking the SEM images of the two sets of hydrogels, five locations were randomly selected and the average pore size was determined (Figure 2F). The results have revealed that the pore sizes of the SF hydrogels (21.50 ± 2.093 μm) and SF/Gel hydrogels (22.01 ± 2.74 μm) were not statistically different. Moreover, the water content (Figure 2G) of SF hydrogels (81.90% ± 2.19%) and SF/Gel hydrogels (81.09% ± 2.23%) showed no statistical difference. These results indicate that both groups scaffolds have high water content and high connectivity, which can provide a suitable extracellular microenvironment for cell proliferation, differentiation and migration, and facilitate the deposition of an ECM.

3.1.2 FTIR spectral analysis

We have applied FTIR spectroscopy to study the removal effect of HFIP by boiling method and the effect of HFIP on hydrogel composition; the associated FTIR spectra are shown in Figure 2C,E. The intensity of peaks associated with the -CF_3 asymmetric bending vibrations peaks (indicated by black arrows) at 1,285 cm^{-1}, 1,181 cm^{-1} and 680 cm^{-1} were significantly reduced following solvent evaporation, as shown in Figure 2E. This indicates an effective removal of HFIP, which has been confirmed by subsequent cytotoxicity tests. After cross-linking with HFIP, the amide I absorption group of 1,636 cm^{-1} in SF shifted to 1,619 cm-1; the amide I absorption group of 1,627 cm^{-1} in Gel shifted to 1,619 cm^{-1}, indicating an increase in β-sheet formation (Zhang et al., 2020). There is minimal impact on amide II (1512 cm^{-1}) before and after cross-linking, suggesting that the hydrogel cross-linking process does not significantly alter other structures. The infrared protein two-dimensional structure analysis map presented in Figure 2D reveals an increase in the β-sheet content in SF/Gel hydrogels compared with SF hydrogels, indicating that the presence of gel materials can increase the β-sheet component.

3.1.3 Mechanical properties

The results of compression and tensile tests are shown in Figure 2H, I, where it can be seen that the compression modulus of the SF (4.61 ± 0.91 MPa) and SF/Gel (4.98 ± 0.99 MPa) groups are very close, and both satisfy the mechanical requirements of articular cartilage. In contrast, the tensile modulus (39.75 ± 6.54 MPa) of the SF/Gel group was higher than the SF gel (24.51 ± 2.07 MPa), which may be attributed to the higher β-sheet content in the SF/Gel.

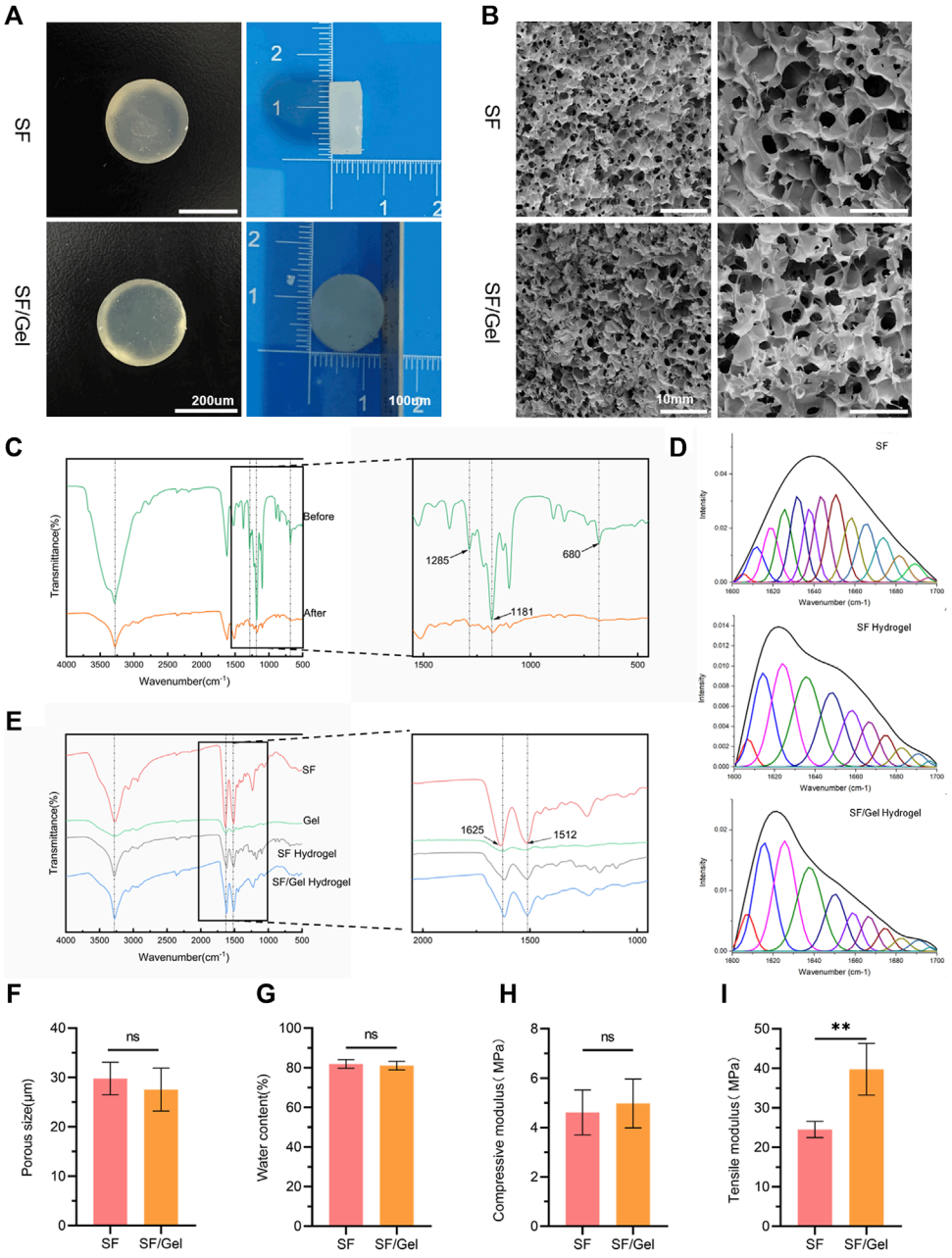

FIGURE 2
Structural characterization of hydrogels. **(A)** Digital photograph of the hydrogels. **(B)** SEM images. **(C)** FTIR spectra of samples before and after HFIP removal. **(D)** Infrared protein secondary structure analysis plots. **(E)** FTIR spectra of samples before and after hydrogel cross-linking. **(F)** Pore size. **(G)** Water content. **(H)** Compression modulus. **(I)** Tensile modulus.

3.2 *In vitro* evaluation of SF/Gel composite hydrogels on AC

3.2.1 Cell adhesion and survival

We first analysed the toxicity of the hydrogel material by culturing AC in the hydrogel extract using CCK-8. The results presented in Figure 3A reveal that the absorbance value for the SF/Gel group (after a 3-day culture) was significantly higher than the SF group and close to the control group. The OD recorded for the SF group was 80% of the control group, indicating no obvious cytotoxicity in SF group. The morphology and attachment of AC to the gels were evaluated using the Actin-Tracker Green-488 (Beyotime China)/DAPI (Beyotime China) method, as shown in Figure 3B. It can be seen that the AC were dispersed on the whole surface of the gel scaffolds for both groups, with a growth status that was good, and the cells showed a typical irregular and raised morphology. This indicates that the hydrogel exhibited good biocompatibility. The live-dead fluorescence staining results for the cells on hydrogels after day 3 (Figure 3D) reveals that AC adhered and grew well on the two hydrogels. Moreover, a calculation of the

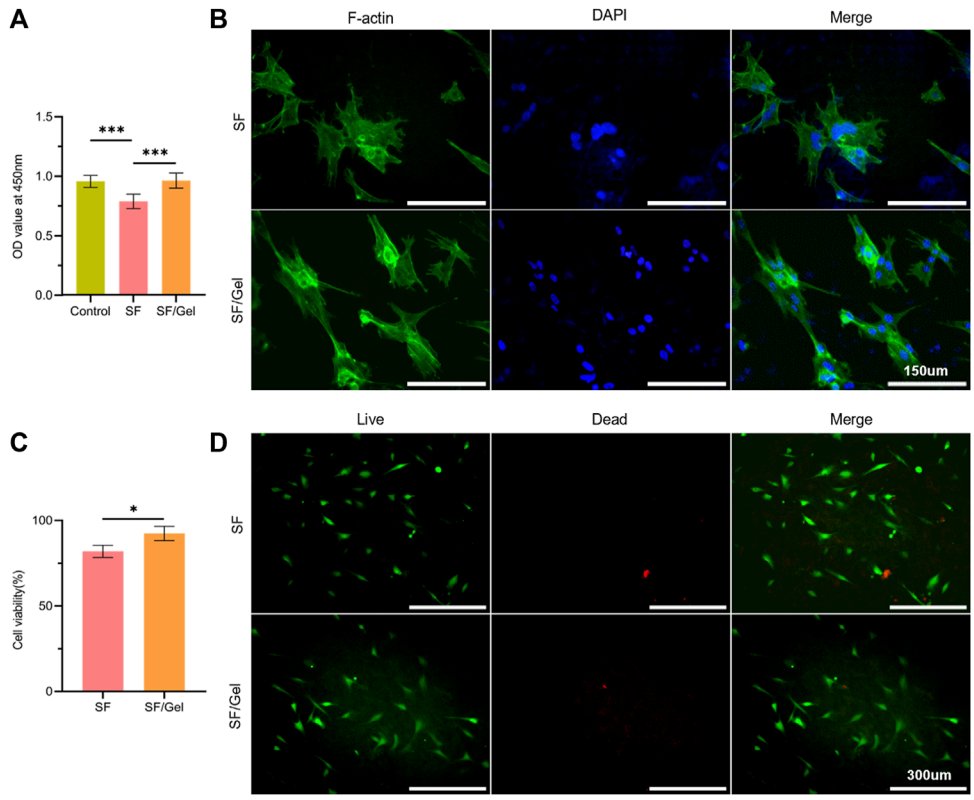

FIGURE 3
In vitro cytotoxicity and adhesion state of AC on scaffolds. **(A)** CCK-8 assays results. **(B)** Immunofluorescence of F-actin cell membrane (green) and DAPI cell nuclear (blue) staining. **(C)** The proportion of live-dead cell areas. **(D)** Calcein-AM/PI live-dead dye staining.

ratio of live to dead cell areas has shown that the dead cell area of the SF/Gel group was smaller than the SF group (Figure 3C).

3.2.2 Cell viability

The metabolic activity of the cells on the hydrogel over 14 days was assessed using Alamar Blue (Figure 4A). There was no significant difference observed for the two hydrogel scaffolds in the culture relative to the control group after days 1, 3, and 5. In contrast, the SF/Gel group exhibited a higher cell viability than the SF gel group after days 7 and 14, combined with good biocompatibility. Both hydrogels supported the proliferation of AC with increasing cell numbers. Cell viability of the SF/Gel group was significantly higher than the SF gel group.

3.2.3 Biochemical analysis

In cartilage regeneration, the production of collagen and GAG is important as both are components of the cartilage ECM (Morgan et al., 2006). We monitored GAG production and HYP levels by AC on hydrogels and normalized the results with respect to DNA content. Over the 14 days of culture, the DNA content of cells in both groups increased after days 3, 5, and 7, but after day 14 the SF/Gel group exhibited significantly more DNA than the SF group (Figure 4B). The deposition of GAG on the SF/Gel hydrogel group was higher after days 5, 7, and 14 (Figure 4C). Moreover, the SF/Gel hydrogel group showed a higher deposition of HYP after days 5 and 7 (Figure 4D). After 14 days of culture, the mRNA (Figure 4E) content of cartilage formation-related genes and the RT-PCR results (Figures 4F–I) reveal that AC on SF/Gel hydrogels exhibited ACAN, COL-1, COL-2 and SOX9 cartilage formation genes, which were significantly elevated relative to the SF hydrogels after 14 days of co-cultivation; this is consistent with GAG and HYP analysis. The results indicate that AC cultured within SF/Gel hydrogels have a strong chondrogenic differentiation capacity, which is demonstrated by the increased production of GAG and HYP as well as the expression of chondrogenic-related genes *in vitro*. In summary, compounding Gel in SF gels in a culture environment can effectively stimulate the production of collagen secreted by AC, providing an ideal platform for articular chondrocyte growth, proliferation, and ECM deposition.

3.3 Repair of *in situ* defects of articular cartilage

In order to evaluate a possible repair effect of two groups hydrogels *in vivo*, we conducted experiments on the repair of a femoral condylar cartilage injury in rabbits. SF hydrogels and SF/Gel hydrogels were implanted into the rabbit medial femoral condylar cartilage defect model, and no hydrogel was implanted as a control group (Figure 5B). Samples were collected 1 month and 2 months following operation for gross observation, imaging, histology and immunohistochemical analysis.

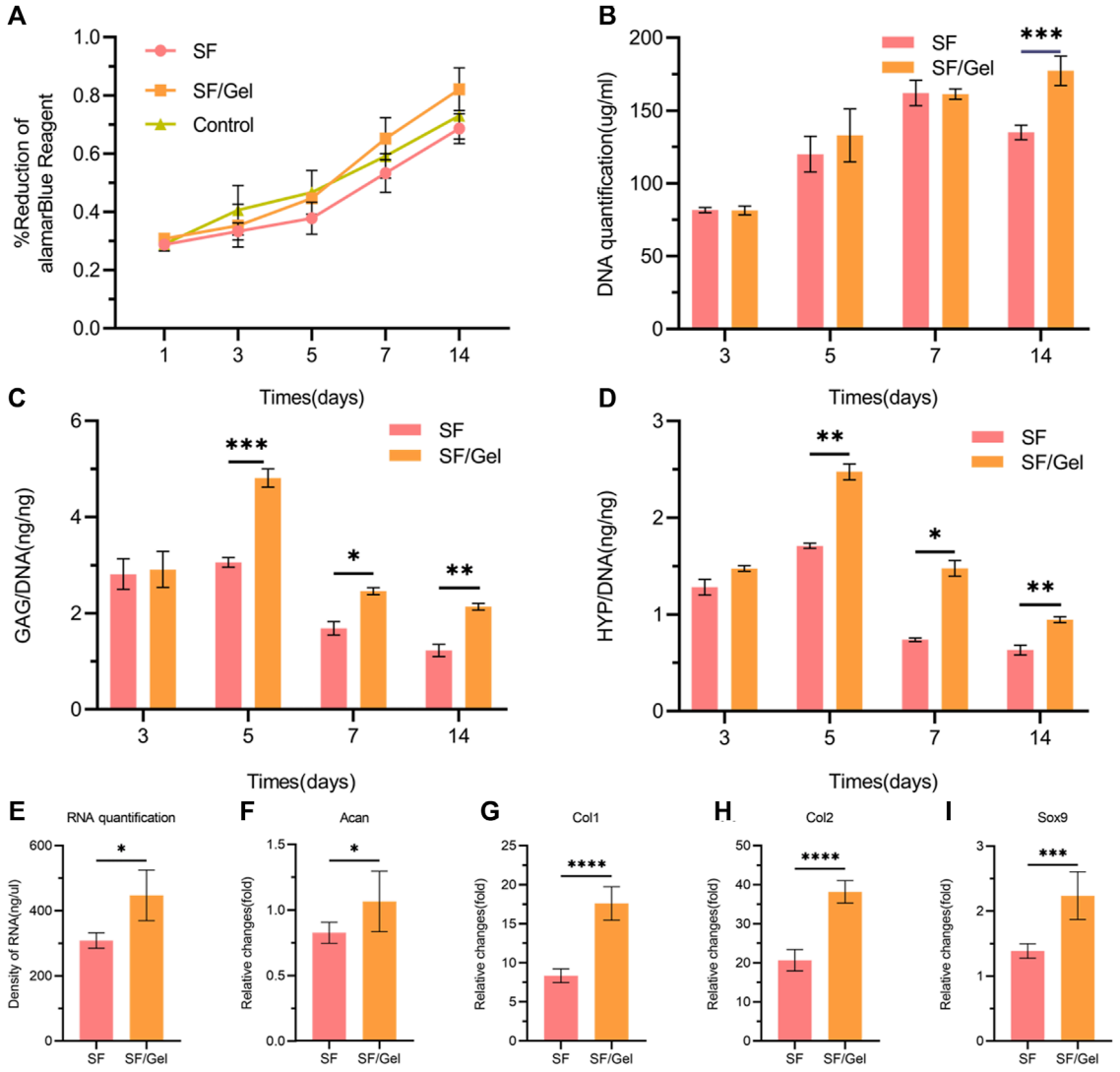

FIGURE 4
In vitro viability and cartilage matrix production of AC on scaffolds. **(A)** Metabolic activity of chondrocytes on different hydrogels. **(B)** DNA content of AC on different hydrogels. **(C, D)** GAG and HYP production by AC on different hydrogels. **(E)** Content of cultured mRNA from articular cartilage on different hydrogels. **(F–I)** Expression of ACAN, COL-1, COL-2 and SOX9 genes in AC on different hydrogels.

3.3.1 Macroscopic analysis

The gross observation is illustrated in Figure 5B. The intraoperative image found that the area and depth of cartilage defects were consistent across the three groups of animals, and the hydrogel material filled the defects effectively. One month post-operation, a significant reduction in the defect area was observed in the control group, but there was still a large area of defects and the defects were deeper. There was a small indentation evident in the SF group. When compared with the two hydrogel groups, the new cartilage in the control group exhibited obvious depressions, and there is an obvious interface between the regenerated tissue and surrounding natural tissues. In the case of the SF/Gel group, there was a greater degree of neocartilage generation, and the articular surface appeared smooth, but the difference in the color of the neocartilage and normal cartilage was quite obvious. Two months after surgery, the control group exhibited more repaired tissue at the cartilage defect, where the new cartilage showed a clear boundary with the surrounding normal cartilage. In the case of the SF group, the new cartilage appeared somewhat degraded and worn, the articular surface was uneven, but the new tissue was still bound to the surrounding normal tissues. The new tissue in the SF/Gel group was smoother, and there was no obvious boundary with the surrounding tissues. According to the ICRS macroscopic scores (Figures 5D,F), for SF (7.33 ± 0.58) and SF/Gel (10.00 ± 1.00) were lower than the control group (3.00 ± 1.00) at month 1; at months 2, the mean scores of the SF (10.33 ± 1.53) and SF/Gel (13.00 ± 1.00) groups were also lower than the control group (7.67 ± 0.58). In a word, the overall repair assessment scores of the SF/Gel group were significantly higher than those of the other groups, one and 2 months following surgery.

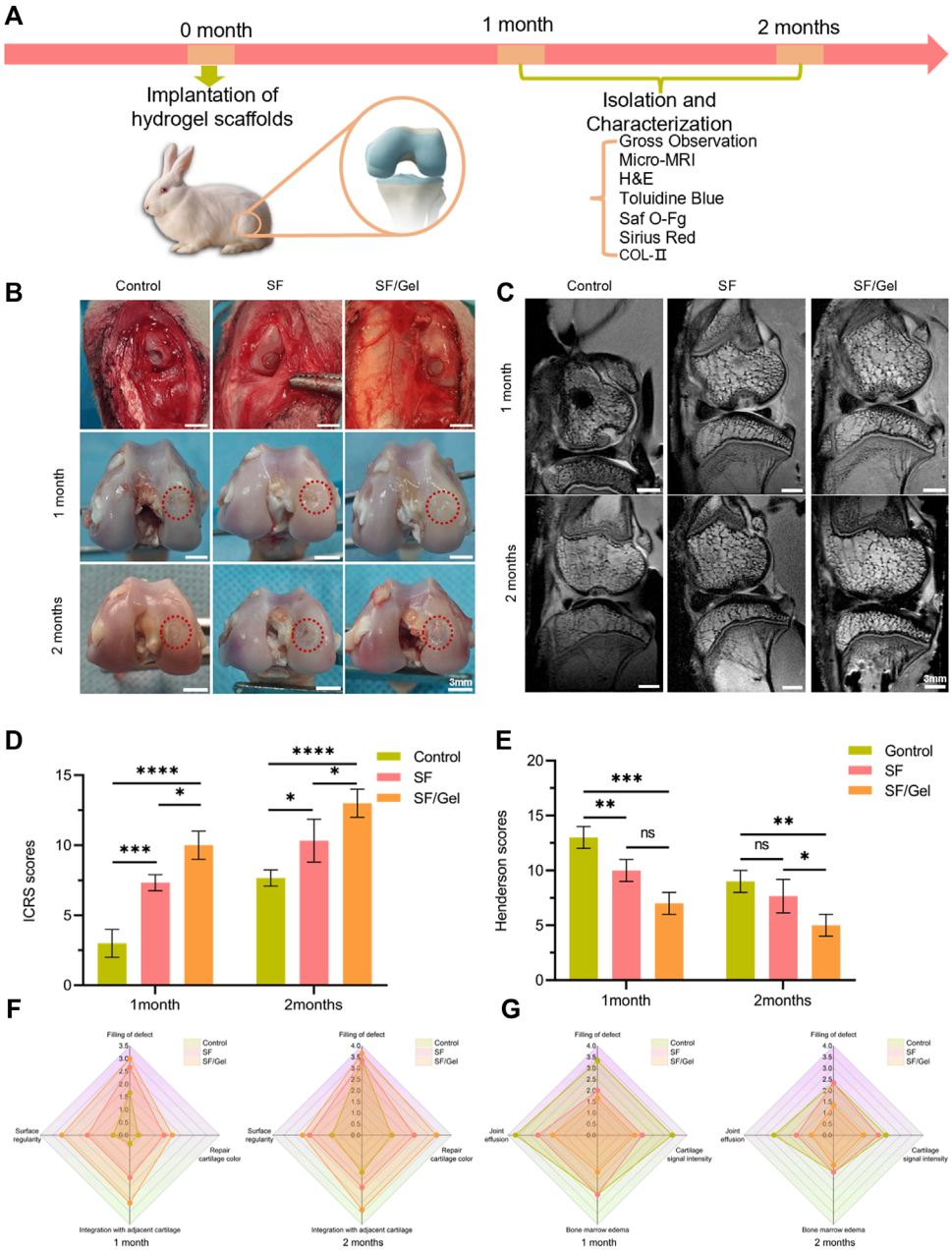

FIGURE 5
The macroscopic morphology, histology and immunohistochemical analysis of rabbit medial condyle cartilage injury and repair. **(A)** The animal experiment process. **(B)** Intraoperative image and gross image (identified by dashed red frames). **(C)** Sagittal MRI pictures. **(D)** Gross view ICRS scores. **(E)** Henderson scores of the MRI. **(F)** The gross view ICRS scores specific distribution. **(G)** The MRI Henderson scores specific distributions.

3.3.2 Imaging evaluation

Micro-MRI scan images have provided an effective visualization of cartilage regeneration. The two-dimensional sagittal images (Figure 5C) show that 1 month after surgery, the amount of newly formed cartilage tissue in the defect area was significantly higher in both the SF group and SF/Gel group compared to the control group, which exhibited more pronounced cartilage defects. Two months post-surgery, significant healing of defects was observed in both experimental groups. The cartilage interface in the SF/gel group appeared smooth and continuous, while in the SF group it was slightly depressed. In contrast, the control group exhibited obvious cartilage defects with a discontinuous interface. Based on the MRI images, the Henderson scores (Figures 5E,G) for SF (9.33 ± 1.53) and SF/Gel (7.00 ± 1.00) were higher than the control group (13.00 ± 1.00) at month 1; at month 2, the mean scores of the SF (7.33 ± 1.53) and SF/Gel (5.00 ± 1.00) groups were also higher than the control group (9.67 ± 1.53).

3.3.3 Histology and immunohistochemical analysis

The area of cartilage defects was evaluated by immunohistochemical staining using H&E, Saf O-Fg, Sirius red and Toluidine Blue and type II collagen immunohistochemical staining. The results of H&E staining at one and 2 month post-operative stages (Figures 6A,B) showed differences in the regenerated cartilage tissue at the defect location for the three groups. In the control group, the formation of fibrous scar tissue was observed with obvious defects. In contrast, cartilage-like tissue was evident in the SF group with disorganized cells, and the new tissue exhibited clear boundaries with the surrounding normal tissues where the thickness of cartilage was thinner. The new cartilage in the SF/Gel group was more obvious, with distinct cartilage tissue characteristics. The GAG distribution in the new cartilage tissue and subchondral bone regeneration were analyzed using Saf O-Fg staining. Sirius red dye is strongly acidic and readily binds to the basic groups in collagen, which is stained red whereas the muscle fibers are stained yellow. Toluidine blue staining was used to detect the presence of proteoglycans in cartilage as it has a high affinity for the sulfate group of proteoglycans. One month post-operation, new cartilage was less evident in the control group and SF group, and the GAG content was smaller when compared with the new cartilage at the center of the defect in the SF/Gel group. After 2 months, the SF/Gel group was characterized by a well-aligned cartilage layer over the intact subchondral bone layer, whereas the SF group showed extensive new cartilage in the subchondral bone with poor subchondral bone formation; the control group still exhibited a significant cartilage defect. Immunohistochemical analysis has demonstrated the expression of collagen in the center of the defect. One month post-operation, the SF/Gel group had produced more neocartilage tissue and the positive expression was obvious, whereas the SF group generated lesser neocartilage and the positive expression of COL-II was weaker than observed for the SF/Gel group. In the case of the control group, the cartilage defects were more obvious, and more chondrocyte-like tissues were produced at the defects, with a stronger positive expression of COL-II. Two months post-operation, the SF/Gel group produced more COL II-rich hyaline-like cartilage. The hyaline cartilage associated with the SF group was thinner with a rough surface and a significant presence of cartilage-like tissue in the subchondral layer. In the case of the control group, the defects were mainly filled with ordinary fibrocartilage with a less obvious COL-II positive expression.

The cartilage defect repair has been quantified by the ICRS-I cartilage repair score (Figures 6C,D). One month post-operation, the scores ($p \leq 0.05$) for the SF/Gel group, control group and SF group were 9.33 ± 2.08, 8.67 ± 1.53 and 4.33 ± 1.16, respectively. Two months post-operation, the scores ($p \leq 0.05$) for the SF/Gel group, SF group and control group were 15.67 ± 0.58, 11.67 ± 1.16 and 6.33 ± 1.53. The higher histologic scores for the SF/Gel group establish better repair results relative to the SF and control groups. A number of studies have demonstrated that SF and Gel promote cartilage repair (Chen et al., 2019; Wu et al., 2020; Li et al., 2021; Zheng et al., 2023). Our results complement that work in confirming defective cartilage repair using the SF group and SF/Gel group materials.

4 Discussion

In the field of tissue engineering, significant efforts have been dedicated to developing an optimal cartilage repair material. This material must possess outstanding biocompatibility, support chondrocyte proliferation, and expedite cartilage repair. In this study, a robust SF/Gel biomaterial hydrogel scaffold was fabricated, comprising two biomaterials known for their favorable cartilage properties. Notably, the biomechanical strength and toughness of this hydrogel scaffold surpass those of conventional hydrogels and synthetic materials with similar properties. Utilizing a rabbit knee cartilage defect model, the study investigated the hydrogel's efficacy in promoting cartilage regeneration *in vivo*.

Using the BSCIT protocol (Zhu Z. et al., 2018), HFIP was employed as a chemical cross-linking agent to enhance the formation of β-sheet secondary structures in SF proteins, resulting in the production of high-strength SF hydrogels. Previous research has indicated that an increased β-sheet content can enhance the biomechanical properties of hydrogel materials. Therefore, the combination of SF and Gel was utilized in this study to further elevate the β-sheet content in the hydrogel, resulting in the development of SF/Gel biomaterial hydrogel with superior biomechanical properties. Through comprehensive characterization testing, *in vitro* biocompatibility assessments, and *in vivo* animal experiments, it was confirmed that the hydrogel not only exhibited exceptional biocompatibility but also effectively promoted the repair of rabbit knee joint cartilage.

In the process of preparing SF hydrogels, the sequence of solvent addition cannot be changed, and DI must be added to the SF/HFIP solvent mixture. Due to its cytotoxic nature, HFIP is not suitable for promoting cell growth. We utilized the low boiling point of HFIP at 59°C to effectively remove the solvent using the evaporation method. While HFIP may be removed by solvent displacement, it is difficult for a solvent to penetrate the dense internal hydrogel structure, so displacement is not an effective option (Zhu Z. et al., 2018). The infrared protein two-dimensional structure analysis reveals an increase in the β-sheet content in SF/Gel hydrogels compared with SF hydrogels, indicating that the presence of gel materials can increase the β-sheet component. This may account for the observation that SF/Gel hydrogel is higher on the tensile modulus than the SF hydrogels. Previous studies have noted that the mechanical properties of hydrogels are enhanced with the addition of Gel that increased β-sheet content (Gil et al., 2005). Taking an overview of the literature, the mechanical properties of hydrogels are closely related to the β-sheet content (Zhu Z. et al., 2018).

In designing hydrogel scaffolds for articular cartilage repair, the mechanical properties of the scaffolds are critical. In natural cartilage tissue, the superficial, middle and deep compression modulus are 0.079 MPa, 2.1 MPa, and 7.75 MPa, respectively (Chen et al., 2001). The results of compression and tensile tests are shown in Figures 2H,I, where it can be seen that the compression modulus of the SF (4.98 ± 0.65 MPa) and SF/Gel (4.60 ± 1.17 MPa) groups are very close, and both satisfy the mechanical requirements of articular cartilage. In contrast, the tensile modulus (39.75 ± 6.54 MPa) of the SF/Gel group was higher than the SF gel (24.51 ± 2.07 MPa), which may be attributed to the higher β-sheet content in the SF/Gel.

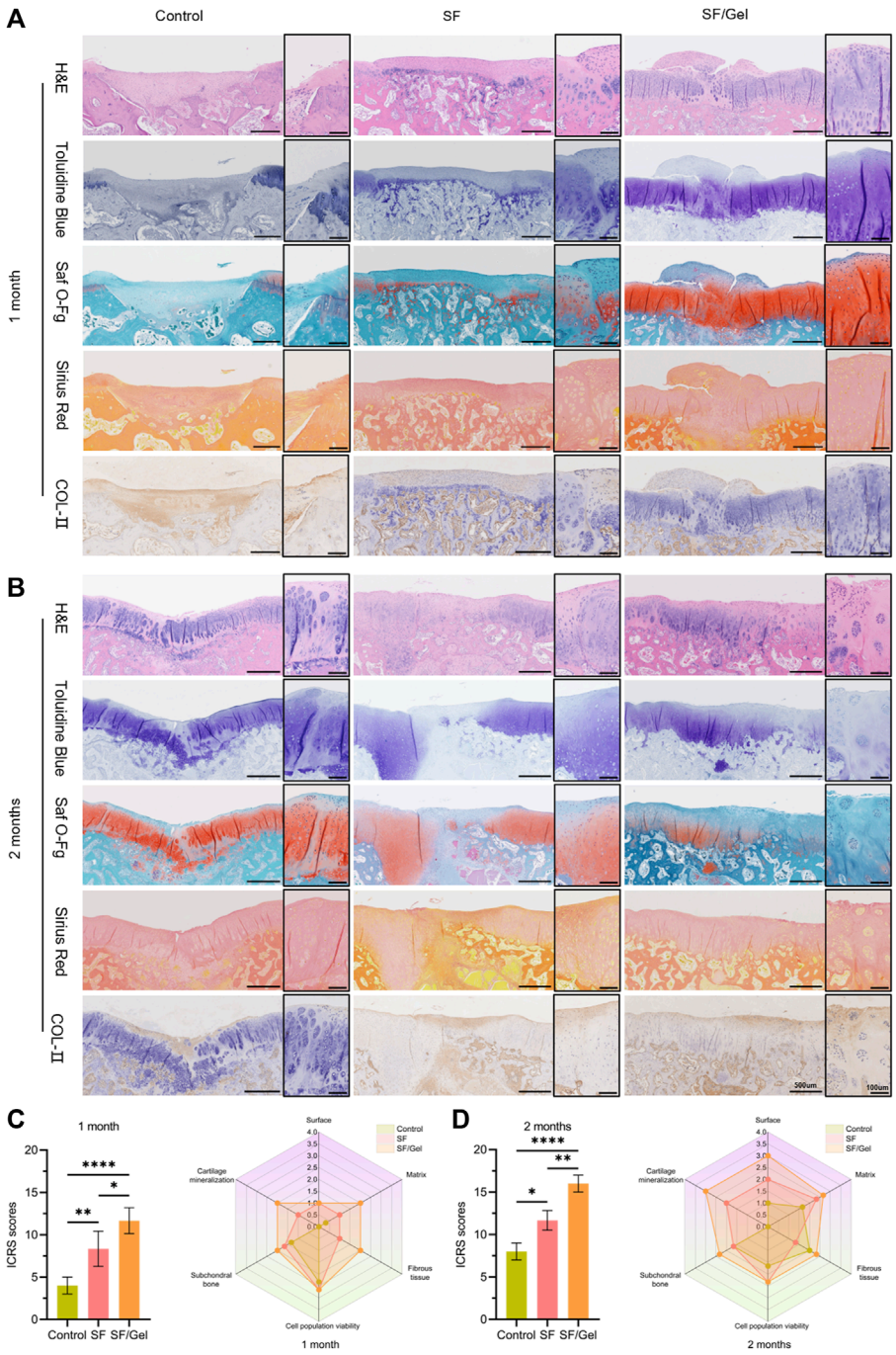

FIGURE 6
Histologic evaluation of regenerated cartilage *in vivo*. **(A, B)** Detection of cartilage damage repair by H&E, Toluidine Blue, Saf O-Fg, Sirius Red and COL-II immunohistochemical staining **(C, D)** Histologic ICRS scores for each group.

The compressive modulus did not show significant improvement, possibly due to the direction of force applied on the hydrogel and the structural orientation of β-sheet (De Leon Rodriguez et al., 2016; Su et al., 2017). The specific reasons behind this phenomenon remain unclear and warrant further investigation. The measured values are higher by orders of magnitude when compared with conventional hydrogels (0.01–0.1 MPa) (Li et al., 2014). Zhu et al. used biomaterials (sodium alginate and bacterial fibres) to prepare a double cross-linked hydrogel with a compression modulus of 0.32 MPa (Zhu X. et al., 2018); Li et al. used synthetic materials (Polyvinyl alcohol and Polyvinylpyrrolidone) to prepare a triple crosslinked hydrogel with a compressive strength of: 4.2 MPa and tensile strength of: 1.92 MPa (Li et al., 2022). In addition, Awasthi et al. used synthetic hydrogels titanium oxide (TiO2), carbon nanotubes (CNTs) and polyacrylamide (PAM) to prepare PAM–TiO2–CNT high-strength hydrogels with compressive

strength and elastic modulus of only 0.43 and 2.340 MPa. However, in this study, the compressive strength and elastic modulus of biomaterial hydrogels were prepared by using biomaterial hydrogels SF and Gel, which far exceeded those of the above synthetic materials (Awasthi et al., 2021). It is worth noting that the mechanical properties of the biomaterial hydrogels prepared in our study surpass those of the majority of hydrogels.

It should be noted that the brittleness of the hydrogel scaffolds increased following HFIP removal, which may be related to the increased presence of DI following solvent evaporation, resulting in an excess β-sheet content (Zhu Z. et al., 2018). We have subjected the hydrogel materials to physical and chemical analysis. However, the loose structure of the hydrogel material that results after repeated freeze-drying caused difficulties in weighing the material and accurately assessing material biodegradability. Consequently, degradation rate tests have not been included in this study. In future work, we will examine the material structure in greater depth in order to overcome this difficulty.

The cytocompatibility and bioactivity of the hydrogel were tested using *in vitro* cultured AC. Gel is a derivative of collagen, which in turn is the main component of cartilage, and has lower antigenicity and good biocompatibility when compared with collagen. It shares common properties with collagen in facilitating cell adhesion and cartilage regeneration, which can be exploited in the repair and regeneration of cartilage tissue. Due to the cytotoxicity of HFIP and the high temperature during solvent evaporation, we were unable to incorporate seed cells or cytokines in this hydrogel. Therefore, future work could find another cross-linking protocol is then required to generate high-strength hydrogels. It has been reported that SF and Gel can promote the secretion of GAG and collagen by chondrocytes (Chen et al., 2019; Wu et al., 2020; Lee et al., 2021; Yuan et al., 2021; Wu et al., 2022; Su et al., 2023; Zheng et al., 2023). Our study is consistent with previous findings that SF material and Gel material promote chondrocytes to produce more ECM deposition relative to the control group; the deposition of GAG and HYP in the SF group was higher than the control group. The incorporation of Gel can promote the GAG and HYP production and increase the expression of related genes.

In this study, a cylindrical cartilage defect with a diameter of 3 mm was utilized in the rabbit animal model for *in vivo* experiments. Cartilage regeneration was quantitatively analyzed 1 month and 2 months post-surgery in each group using Henderson MRI evaluation criteria, ICRS Macroscopic Evaluation Scale, and the ICRS repair tissue assessment scoring criteria. The results indicated that both the SF/Gel group and the SF group exhibited significant cartilage regeneration ability (Figure 5; Figure 6). Furthermore, the defect filling, histological staining, and COL-II staining of the SF/Gel group demonstrated superior results compared to those of the SF group, indicating an excellent cartilage regeneration effect. These findings emphasize that the combination with Gel is crucial for achieving the most remarkable cartilage regeneration ability and effectively promoting cartilage repair in the body.

The above test results demonstrate that SF/Gel hydrogels can promote the proliferation of AC and deposition of extracellular cartilage matrix, which ultimately facilitates the repair of articular cartilage injuries. However, there are three limitations that must be addressed. 1) Although HFIP is effectively removed by solvent evaporation, this treatment results in a brittle hydrogel. 2) The balance between hydrogel degradation and the regenerative microenvironment of the nascent tissues requires further exploration. 3) The mechanism involved in the SF/Gel hydrogel promotion of chondrocytes to produce more cartilage ECM warrants further study.

Biomaterial hydrogels are known for their good biocompatibility, but often fall short in meeting the biomechanical requirements of articular cartilage. To address this issue, we combined SF and Gel) both biomaterials, and utilized the BSICT cross-linking scheme to develop a hydrogel with exceptional toughness and strength. Through experimental validation, we confirmed that this hydrogel surpasses similar biomaterial hydrogels in biomechanical properties, effectively meeting the stress demands of articular cartilage. Furthermore, our research revealed that the hydrogel not only enhances the proliferation of articular cartilage cells and ECM production but also facilitates the regeneration and repair of articular cartilage defects in rabbit models. This innovative hydrogel not only addresses the biomechanical limitations of biomaterial hydrogels but also retains their excellent biocompatibility. Our findings suggest a promising model for the utilization of high-strength hydrogels in soft tissue regeneration and offer a new avenue for cartilage defect treatment, bridging the gap between basic research and clinical application.

5 Conclusion

The high-strength SF/Gel hydrogel prepared using the BSICT protocol demonstrates superior mechanical properties, addressing the limitations of biomaterial hydrogels. By combining SF with HFIP in a 0.8 (g): 3 (mL) ratio and incorporating a 2% Gel solution to enhance β-sheet formation, we achieved high-strength hydrogels. The tensile modulus of the SF/Gel group (39.75 ± 6.54 MPa) surpassed that of the SF group (24.51 ± 2.07 MPa), indicating that the presence of β-sheet content significantly enhanced the hydrogel's mechanical properties. Additionally, the SF/Gel hydrogel maintained normal chondrocyte phenotype, stimulating ECM production and facilitating cartilage defect repair to mitigate osteoarthritis effects. The exceptional mechanical properties and biocompatibility of this hydrogel position it as a promising material for knee joint cartilage repair, offering a viable approach for articular cartilage regeneration and advancements in tissue engineering.

Data availability statement

The raw data supporting the conclusion of this article will be made available by the authors, without undue reservation.

Ethics statement

The animal study was approved by the Institutional Animal Care and Use Committee of Beijing Keyu. The study was conducted in accordance with the local legislation and institutional requirements.

Author contributions

HM: Data curation, Methodology, Validation, Writing–original draft, Writing–review and editing. BX: Methodology, Resources, Writing–original draft. HC: Conceptualization, Supervision, Writing–review and editing. PS: Visualization, Writing–review and editing. YZ: Data curation, Writing–original draft. HJ: Investigation, Writing–original draft. JL: Resources, Writing–original draft. YZ: Project administration, Supervision, Writing–original draft, Writing–review and editing. YZ: Conceptualization, Funding acquisition, Methodology, Writing–original draft, Writing–review and editing.

Funding

The author(s) declare that financial support was received for the research, authorship, and/or publication of this article. This work was supported by the National Natural Science Foundation of China (82072451), the Research and Translational Application of Clinical Characteristic Diagnosis and Treatment Techniques in the Capital (Z221100007422014) and the Natural Science Foundation of Beijing (7202199).

Conflict of interest

The authors declare that the research was conducted in the absence of any commercial or financial relationships that could be construed as a potential conflict of interest.

Publisher's note

All claims expressed in this article are solely those of the authors and do not necessarily represent those of their affiliated organizations, or those of the publisher, the editors and the reviewers. Any product that may be evaluated in this article, or claim that may be made by its manufacturer, is not guaranteed or endorsed by the publisher.

Supplementary material

The Supplementary Material for this article can be found online at: https://www.frontiersin.org/articles/10.3389/fmats.2024.1390372/full#supplementary-material

References

Abpeikar, Z., Moradi, L., Javdani, M., Kargozar, S., Soleimannejad, M., Hasanzadeh, E., et al. (2021). Characterization of macroporous polycaprolactone/silk fibroin/gelatin/ascorbic acid composite scaffolds and *in vivo* results in a rabbit model for meniscus cartilage repair. *Cartilage* 13 (2_Suppl. l), 1583s–1601s. doi:10.1177/19476035211035418

Awasthi, S., Gaur, J. K., Pandey, S. K., Bobji, M. S., and Srivastava, C. (2021). High-strength, strongly bonded nanocomposite hydrogels for cartilage repair. *ACS Appl. Mater Interfaces* 13 (21), 24505–24523. doi:10.1021/acsami.1c05394

Brown, W. E., Potter, H. G., Marx, R. G., Wickiewicz, T. L., and Warren, R. F. (2004). Magnetic resonance imaging appearance of cartilage repair in the knee. *Clin. Orthop. Relat. Res.* 422, 214–223. doi:10.1097/01.blo.0000129162.36302.4f

Budharaju, H., Chandrababu, H., Zennifer, A., Chellappan, D., Sethuraman, S., and Sundaramurthi, D. (2024). Tuning thermoresponsive properties of carboxymethyl cellulose (CMC)-agarose composite bioinks to fabricate complex 3D constructs for regenerative medicine. *Int. J. Biol. Macromol.* 260 (Pt 1), 129443. doi:10.1016/j.ijbiomac.2024.129443

Buyanov, A. L., Gofman, I. V., and Saprykina, N. N. (2019). High-strength cellulose-polyacrylamide hydrogels: mechanical behavior and structure depending on the type of cellulose. *J. Mech. Behav. Biomed. Mater* 100, 103385. doi:10.1016/j.jmbbm.2019.103385

Chahla, J., Sweet, M. C., Okoroha, K. R., Nwachukwu, B. U., Hinckel, B., Farr, J., et al. (2019). Osteochondral allograft transplantation in the patellofemoral joint: a systematic review. *Am. J. Sports Med.* 47 (12), 3009–3018. doi:10.1177/0363546518814236

Chen, H. C., Chang, Y. H., Chuang, C. K., Lin, C. Y., Sung, L. Y., Wang, Y. H., et al. (2009). The repair of osteochondral defects using baculovirus-mediated gene transfer with de-differentiated chondrocytes in bioreactor culture. *Biomaterials* 30 (4), 674–681. doi:10.1016/j.biomaterials.2008.10.017

Chen, S. S., Falcovitz, Y. H., Schneiderman, R., Maroudas, A., and Sah, R. L. (2001). Depth-dependent compressive properties of normal aged human femoral head articular cartilage: relationship to fixed charge density. *Osteoarthr. Cartil.* 9 (6), 561–569. doi:10.1053/joca.2001.0424

Chen, Y., Wu, T., Huang, S., Suen, C. W., Cheng, X., Li, J., et al. (2019). Sustained release SDF-1α/TGF-β1-loaded silk fibroin-porous gelatin scaffold promotes cartilage repair. *ACS Appl. Mater Interfaces* 11 (16), 14608–14618. doi:10.1021/acsami.9b01532

Cui, S., Zhang, S., and Coseri, S. (2023). An injectable and self-healing cellulose nanofiber-reinforced alginate hydrogel for bone repair. *Carbohydr. Polym.* 300, 120243. doi:10.1016/j.carbpol.2022.120243

De Leon Rodriguez, L. M., Hemar, Y., Cornish, J., and Brimble, M. A. (2016). Structure–mechanical property correlations of hydrogel forming β-sheet peptides. *Chem. Soc. Rev.* 45 (17), 4797–4824. doi:10.1039/c5cs00941c

Fiocco, L., Li, S., Stevens, M. M., Bernardo, E., and Jones, J. R. (2017). Biocompatibility and bioactivity of porous polymer-derived Ca-Mg silicate ceramics. *Acta Biomater.* 50, 56–67. doi:10.1016/j.actbio.2016.12.043

Gan, S., Lin, W., Zou, Y., Xu, B., Zhang, X., Zhao, J., et al. (2020). Nano-hydroxyapatite enhanced double network hydrogels with excellent mechanical properties for potential application in cartilage repair. *Carbohydr. Polym.* 229, 115523. doi:10.1016/j.carbpol.2019.115523

Gil, E. S., Spontak, R. J., and Hudson, S. M. (2005). Effect of β-sheet crystals on the thermal and rheological behavior of protein-based hydrogels derived from gelatin and silk fibroin. *Macromol. Biosci.* 5 (8), 702–709. doi:10.1002/mabi.200500076

Gong, D., Lin, Q., Shao, Z., Chen, X., and Yang, Y. (2020). Preparing 3D-printable silk fibroin hydrogels with robustness by a two-step crosslinking method. *RSC Adv.* 10 (45), 27225–27234. doi:10.1039/d0ra04789a

Kapoor, S., and Kundu, S. C. (2016). Silk protein-based hydrogels: promising advanced materials for biomedical applications. *Acta Biomater.* 31, 17–32. doi:10.1016/j.actbio.2015.11.034

Krishnan, Y., and Grodzinsky, A. J. (2018). Cartilage diseases. *Matrix Biol.* 71-72, 51–69. doi:10.1016/j.matbio.2018.05.005

Le, H., Xu, W., Zhuang, X., Chang, F., Wang, Y., and Ding, J. (2020). Mesenchymal stem cells for cartilage regeneration. *J. Tissue Eng.* 11, 204173142094383. doi:10.1177/2041731420943839

Lee, S., Choi, J., Youn, J., Lee, Y., Kim, W., Choe, S., et al. (2021). Development and evaluation of gellan gum/silk fibroin/chondroitin sulfate ternary injectable hydrogel for cartilage tissue engineering. *Biomolecules* 11 (8), 1184. doi:10.3390/biom11081184

Li, J., Illeperuma, W. R. K., Suo, Z., and Vlassak, J. J. (2014). Hybrid hydrogels with extremely high stiffness and toughness. *ACS Macro Lett.* 3 (6), 520–523. doi:10.1021/mz5002355

Li, K. W., Klein, T. J., Chawla, K., Nugent, G. E., Bae, W. C., and Sah, R. L. (2004). *In vitro* physical stimulation of tissue-engineered and native cartilage. *Methods Mol. Med.* 100, 325–352. doi:10.1385/1-59259-810-2:325

Li, Q., Xu, S., Feng, Q., Dai, Q., Yao, L., Zhang, Y., et al. (2021). 3D printed silk-gelatin hydrogel scaffold with different porous structure and cell seeding strategy for cartilage regeneration. *Bioact. Mater* 6 (10), 3396–3410. doi:10.1016/j.bioactmat.2021.03.013

Li, W., Qiao, K., Zheng, Y., Yan, Y., Xie, Y., Liu, Y., et al. (2022). Preparation, mechanical properties, fatigue and tribological behavior of double crosslinked high strength hydrogel. *J. Mech. Behav. Biomed. Mater* 126, 105009. doi:10.1016/j.jmbbm.2021.105009

Li, X., Qin, H., Zhang, X., and Guo, Z. (2019). Triple-network hydrogels with high strength, low friction and self-healing by chemical-physical crosslinking. *J. Colloid Interface Sci.* 556, 549–556. doi:10.1016/j.jcis.2019.08.100

Li, Z., Wu, N., Cheng, J., Sun, M., Yang, P., Zhao, F., et al. (2020). Biomechanically, structurally and functionally meticulously tailored polycaprolactone/silk fibroin scaffold for meniscus regeneration. *Theranostics* 10 (11), 5090–5106. doi:10.7150/thno.44270

Lien, S. M., Ko, L. Y., and Huang, T. J. (2009). Effect of pore size on ECM secretion and cell growth in gelatin scaffold for articular cartilage tissue engineering. *Acta Biomater.* 5 (2), 670–679. doi:10.1016/j.actbio.2008.09.020

Liu, H., Cheng, Y., Chen, J., Chang, F., Wang, J., Ding, J., et al. (2018). Component effect of stem cell-loaded thermosensitive polypeptide hydrogels on cartilage repair. *Acta Biomater.* 73, 103–111. doi:10.1016/j.actbio.2018.04.035

Luo, C., Guo, A., Zhao, Y., and Sun, X. (2022). A high strength, low friction, and biocompatible hydrogel from PVA, chitosan and sodium alginate for articular cartilage. *Carbohydr. Polym.* 286, 119268. doi:10.1016/j.carbpol.2022.119268

Mainil-Varlet, P., Aigner, T., Brittberg, M., Bullough, P., Hollander, A., Hunziker, E., et al. (2003). Histological assessment of cartilage repair: a report by the histology endpoint committee of the international cartilage repair society (ICRS). *J. Bone Jt. Surg. Am.* 85 (A Suppl. 2), 45–57. doi:10.2106/00004623-200300002-00007

Morgan, T. G., Rowan, A. D., Dickinson, S. C., Jones, D., Hollander, A. P., Deehan, D., et al. (2006). Human nasal cartilage responds to oncostatin M in combination with interleukin 1 or tumour necrosis factor alpha by the release of collagen fragments via collagenases. *Ann. Rheum. Dis.* 65 (2), 184–190. doi:10.1136/ard.2004.033480

Ni, X., Xing, X., Deng, Y., and Li, Z. (2023). Applications of stimuli-responsive hydrogels in bone and cartilage regeneration. *Pharmaceutics* 15 (3), 982. doi:10.3390/pharmaceutics15030982

Rockwood, D. N., Preda, R. C., Yücel, T., Wang, X., Lovett, M. L., and Kaplan, D. L. (2011). Materials fabrication from *Bombyx mori* silk fibroin. *Nat. Protoc.* 6 (10), 1612–1631. doi:10.1038/nprot.2011.379

Sánchez-Téllez, D. A., Téllez-Jurado, L., and Rodríguez-Lorenzo, L. M. (2017). Hydrogels for cartilage regeneration, from polysaccharides to hybrids. *Polym. (Basel)* 9 (12), 671. doi:10.3390/polym9120671

Schneider, M. C., Chu, S., Randolph, M. A., and Bryant, S. J. (2019). An *in vitro* and *in vivo* comparison of cartilage growth in chondrocyte-laden matrix metalloproteinase-sensitive poly(ethylene glycol) hydrogels with localized transforming growth factor β3. *Acta Biomater.* 93, 97–110. doi:10.1016/j.actbio.2019.03.046

Sheehy, E. J., Mesallati, T., Vinardell, T., and Kelly, D. J. (2015). Engineering cartilage or endochondral bone: a comparison of different naturally derived hydrogels. *Acta Biomater.* 13, 245–253. doi:10.1016/j.actbio.2014.11.031

Shi, R., Huang, Y., Ma, C., Wu, C., and Tian, W. (2019). Current advances for bone regeneration based on tissue engineering strategies. *Front. Med.* 13 (2), 160–188. doi:10.1007/s11684-018-0629-9

Sornkamnerd, S., Okajima, M. K., and Kaneko, T. (2017). Tough and porous hydrogels prepared by simple lyophilization of LC gels. *ACS Omega* 2 (8), 5304–5314. doi:10.1021/acsomega.7b00602

Su, D., Yao, M., Liu, J., Zhong, Y., Chen, X., and Shao, Z. (2017). Enhancing mechanical properties of silk fibroin hydrogel through restricting the growth of β-sheet domains. *ACS Appl. Mater Interfaces* 9 (20), 17489–17498. doi:10.1021/acsami.7b04623

Su, X., Wei, L., Xu, Z., Qin, L., Yang, J., Zou, Y., et al. (2023). Evaluation and application of silk fibroin based biomaterials to promote cartilage regeneration in osteoarthritis therapy. *Biomedicines* 11 (8), 2244. doi:10.3390/biomedicines11082244

Thomas, V., and Mercuri, J. (2023). *In vitro* and *in vivo* efficacy of naturally derived scaffolds for cartilage repair and regeneration. *Acta Biomater.* 171, 1–18. doi:10.1016/j.actbio.2023.09.008

Wakitani, S., Goto, T., Pineda, S. J., Young, R. G., Mansour, J. M., Caplan, A. I., et al. (1994). Mesenchymal cell-based repair of large, full-thickness defects of articular cartilage. *J. Bone Jt. Surg. Am.* 76 (4), 579–592. doi:10.2106/00004623-199404000-00013

Wu, T., Chen, Y., Liu, W., Tong, K. L., Suen, C. W., Huang, S., et al. (2020). Ginsenoside Rb1/TGF-β1 loaded biodegradable silk fibroin-gelatin porous scaffolds for inflammation inhibition and cartilage regeneration. *Mater Sci. Eng. C Mater Biol. Appl.* 111, 110757. doi:10.1016/j.msec.2020.110757

Wu, Y., Zhou, L., Li, Y., and Lou, X. (2022). Osteoblast-derived extracellular matrix coated PLLA/silk fibroin composite nanofibers promote osteogenic differentiation of bone mesenchymal stem cells. *J. Biomed. Mater Res. A* 110 (3), 525–534. doi:10.1002/jbm.a.37302

Wubneh, A., Tsekoura, E. K., Ayranci, C., and Uludağ, H. (2018). Current state of fabrication technologies and materials for bone tissue engineering. *Acta Biomater.* 80, 1–30. doi:10.1016/j.actbio.2018.09.031

Yuan, T., Li, Z., Zhang, Y., Shen, K., Zhang, X., Xie, R., et al. (2021). Injectable ultrasonication-induced silk fibroin hydrogel for cartilage repair and regeneration. *Tissue Eng. Part A* 27 (17-18), 1213–1224. doi:10.1089/ten.TEA.2020.0323

Zhang, W., Chen, J., Qu, M., Backman, L. J., Zhang, A., Liu, H., et al. (2020). Sustained release of TPCA-1 from silk fibroin hydrogels preserves keratocyte phenotype and promotes corneal regeneration by inhibiting interleukin-1β signaling. *Adv. Healthc. Mater* 9 (17), e2000591. doi:10.1002/adhm.202000591

Zhang, X., Zhang, W., and Yang, M. (2018). Application of hydrogels in cartilage tissue engineering. *Curr. Stem Cell Res. Ther.* 13 (7), 497–516. doi:10.2174/1574888x12666171017160323

Zhang, Y., Li, Z., Guan, J., Mao, Y., and Zhou, P. (2021). Hydrogel: a potential therapeutic material for bone tissue engineering. *AIP Adv.* 11, 010701. doi:10.1063/5.0035504

Zhang, Y., Liu, X., Zeng, L., Zhang, J., Zuo, J., Zou, J., et al. (2019a). Polymer fiber scaffolds for bone and cartilage tissue engineering. *Adv. Funct. Mater.* 29 (36), 1903279. doi:10.1002/adfm.201903279

Zhang, Y., Yu, J., Ren, K., Zuo, J., Ding, J., and Chen, X. (2019b). Thermosensitive hydrogels as scaffolds for cartilage tissue engineering. *Biomacromolecules* 20 (4), 1478–1492. doi:10.1021/acs.biomac.9b00043

Zheng, K., Zheng, X., Yu, M., He, Y., and Wu, D. (2023). BMSCs-seeded interpenetrating network GelMA/SF composite hydrogel for articular cartilage repair. *J. Funct. Biomater.* 14 (1), 39. doi:10.3390/jfb14010039

Zhou, K., Ding, R., Tao, X., Cui, Y., Yang, J., Mao, H., et al. (2023). Peptide-dendrimer-reinforced bioinks for 3D bioprinting of heterogeneous and biomimetic *in vitro* models. *Acta Biomater.* 169, 243–255. doi:10.1016/j.actbio.2023.08.008

Zhu, J., and Marchant, R. E. (2011). Design properties of hydrogel tissue-engineering scaffolds. *Expert Rev. Med. Devices* 8 (5), 607–626. doi:10.1586/erd.11.27

Zhu, X., Chen, T., Feng, B., Weng, J., Duan, K., Wang, J., et al. (2018a). Biomimetic bacterial cellulose-enhanced double-network hydrogel with excellent mechanical properties applied for the osteochondral defect repair. *ACS Biomater. Sci. Eng.* 4 (10), 3534–3544. doi:10.1021/acsbiomaterials.8b00682

Zhu, Z., Ling, S., Yeo, J., Zhao, S., Tozzi, L., Buehler, M. J., et al. (2018b). High-strength, durable all-silk fibroin hydrogels with versatile processability toward multifunctional applications. *Adv. Funct. Mater* 28 (10), 1704757. doi:10.1002/adfm.201704757